Ion implantation of germanium into silicon for critical coupling control of racetrack resonators

Milan M. Milosevic[1], Xia Chen[1], Xingshi Yu[1], Nicholas J. Dinsdale[1,2], Ozan Aktas[1], Swe Zin Oo[1,3], Ali Z. Khokhar[1], David J. Thomson[1], Otto L. Muskens[2], Harold M. H. Chong[3], Anna C. Peacock[1], Shinichi Saito[3], Graham T. Reed[1]

[1]*Zepler Institute for Photonics and Nanoelectronics, Optoelectronics Research Centre, University of Southampton, UK*

[2]*Department of Physics and Astronomy, University of Southampton, UK*

[3]*Sustainable Electronic Technologies, Electronics and Computer Science, University of Southampton, UK*

***Abstract*— Critical coupling control is an important concept used in integrated photonics to obtain functionalities such as single and coupled resonator optical filters and wavelength multiplexers. Realization of critical coupling depends strongly on device fabrication, and reproducibility is therefore an ongoing challenge. Post-fabrication trimming offers a solution for achieving optimal performance for individual devices. Ion implantation into silicon causes crystalline lattice damage which results in an increase of the material's refractive index and therefore creates a platform for realization of various optical devices. In recent years, we have presented results on the development of erasable gratings, optical filters and Mach-Zehnder interferometers using ion implantation of germanium into silicon. Here, we report the design, fabrication and testing of silicon-on-insulator racetrack resonators, trimmed by localised annealing of germanium ion implanted silicon using continuous and pulsed wave laser sources. The results demonstrate the ability to permanently tune the critical coupling condition of racetrack resonators. Compared to the pulsed lasers used for annealing, continuous wave lasers revealed much higher extinction ratio due to improved material quality after silicon recrystallization.**

***Index Terms*—Ion implantation, laser annealing, optical filters, racetrack resonators, silicon photonics, trimming.**

I. INTRODUCTION

Silicon photonics has emerged as one of the most buoyant technologies in the world with a broad academic and industrial community worldwide investing significant resources to find low cost solutions for short reach interconnects for data-communications, biomedical and chemical sensing, and healthcare [1-10]. The attractiveness of the silicon-on-insulator (SOI) platform can be mainly attributed to the high refractive index contrast between the silicon core and silicon-dioxide cladding, which enables the possibility of achieving high device density per unit chip area. Additionally, this technology is compatible with the complementary-metal-oxide-semiconductor (CMOS) infrastructure already in existence for the electronics industry, and is expected to improve performance and reliability of electronic circuits and systems by reducing the footprint, power consumption and costs [1].

Recently, there have been many advances in fabrication and processing technology, and exploitation of different material platforms and wavelength ranges. Propagation losses of submicron rib and strip waveguides were reduced to 0.1 dB/cm and 0.7 dB/cm, respectively [11]. The racetrack/ring resonator is one of the fundamental building components of photonic circuits. It is widely used for a variety of applications including areas of spectral filtering, switching and optical delay lines. As a passive optical component, it is also used for a variety of sensing applications such as bio-chemical and strain sensing due to its resonant wavelength sensitivity to a presence of different biomolecules or mechanical stress, respectively.

The racetrack/ring resonator is also used in a variety of active devices acting as a laser, modulator or resonant detector, aiming to provide high compactness and low energy consumption. However, the device is highly sensitive to fabrication errors and ambient temperature fluctuations, making it challenging to achieve accurate control and stability of the resonant wavelength peak and extinction ratio. A micro-heater or thermoelectric cooler is often used to tune the operating wavelength of racetrack/ring resonators via the thermo-optic effect, however this increases the total energy consumption and control complexity of the circuit. Standard configurations, which involve depositing silicon dioxide (~1 μm) on top of the waveguide (between the waveguide and a metal heater), revealed tuning efficiencies in the range of 42 mW/FSR and 100 mW/FSR (FSR - free spectral range) [5], while the use of transparent graphene nano-heaters further increased tuning efficiency achieving 2.4 mW/FSR [5] and ~0.48 nm/mW [6], respectively. Post-fabrication trimming techniques, which don't involve any active tuning, have been investigated worldwide to reduce large resonant wavelength shifts caused by fabrication uncertainties and wafer thickness variations. Electron beam induced compaction and strain to the oxide cladding revealed a very small tuning range (4.9 nm) [7], while electron beam bleaching of a polymer cladding provided even lower tuning range (2 nm) and lacked standard CMOS compatibility [8]. Both methods provide very small refractive index change, resulting in a small tuning range. Additionally, the process is relatively slow (low throughput: >8hours/wafer) and consequentially adds to the fabrication costs. Recently, Spector et al. [9] and Hagan et al. [10] used electrical annealing in the form of an integrated micro-heater to perform resonant wavelength trimming of silicon ring resonators, however their

approach required the cladding material modification or high energy (3 MeV) boron ion implantation of the entire sample which may affect the performance of other optical components located on the same wafer.

Ion implantation into silicon represents a promising platform to demonstrate a variety of optical devices including the post-fabrication trimming of optical filters [10-16]. The level of radiation damage will depend on the type of ions used for implantation and other implantation parameters such as ion-energy and fluence. Depending on these parameters, complete or partial amorphisation can be achieved in localised implanted regions of the device. Amorphous silicon has a higher refractive index than crystalline silicon (Δn=0.5), which can be efficiently tuned using localized laser annealing. Silicon ion implantation has already been used for tuning the resonant wavelength of silicon-on-insulator racetrack resonators [12]. However, high optical losses, low trimming range (~3 nm), poor extinction ratio and low quality factor (Q) were reported. We have recently reported results using Ge-ion implantation technology to trim SOI ring resonators and Mach-Zehnder interferometers in the real-time [13-16].

In our previous papers [1, 2], we examined the potential of various elements, such as germanium, silicon, carbon, tin and xenon, to be used for silicon ion implantation. Germanium ion implantation into silicon was used to introduce lattice disorder because germanium is a group IV material and its use for ion implantation into silicon causes no doping effect in silicon. Germanium is also a CMOS compatible material which possesses higher atomic mass than silicon. This means that similar radiation damage (corresponding to similar refractive index change of silicon) can be achieved using a relatively low implantation dose (~10^{15} Ge-ions/cm^2) enabling reduction of the processing cost and time. Additionally, the implantation process can be carried out at room temperature which is important as there is no self-annealing of the amorphous material during implantation process and a good amorphisation profile can be achieved [1]. The refractive index change is reversible and can be adjusted by selective local annealing to tune the operating performance of silicon photonic devices. In typical applications, it is anticipated that most photonic chips with racetrack resonators will need to operate at a precise temperature which is enabled by external thermal control. In our previous work [13], we used Ge-ion implantation technique to form a short implanted waveguide section (~6 µm) in the silicon waveguide arc of the ring resonator. The results revealed the possibility to trim the resonant wavelength at the designed working temperature, and to compensate for errors in the fabrication process. In this paper, we use the same technique to implant the silicon slab layer located between the bus waveguide and the racetrack in order to control the critical coupling of this device, via controlled partial annealing of the implanted region.

II. DESIGN AND FABRICATION

The transmission spectrum of a racetrack resonator depends on the operating wavelength, mode effective index, the optical path length, and both the self and cross coupling coefficient of the coupler. The coupling efficiency of a racetrack/ring resonator depends on the propagation loss in the resonator and the coupling coefficients, while the mode effective index depends on the refractive index of the material, the waveguide geometry, operating wavelength and ambient temperature [3, 17]. By carrying out ion-implantation of the silicon slab layer in between the bus waveguide and the racetrack, the refractive index of the silicon material can be modified, which induces a change in the critical coupling condition (a point of resonance at which cross-coupling coefficient matches the round trip loss of the resonator). Lumerical Mode Solutions software [18] was used to design silicon rib waveguides and racetrack resonators. Standard 220 nm SOI wafers on a 2 µm buried oxide layer have been used for device fabrication. Silicon rib waveguides were 500 nm wide and contained 100 nm thick silicon slab layer (120 nm silicon etch depth). The racetrack resonators comprised the radius of 25 µm, coupling length of 10 µm and an edge-to-edge waveguide spacing of 260 nm (Fig. 1). We have also fabricated un-implanted racetrack resonators with the same dimensions for reference.

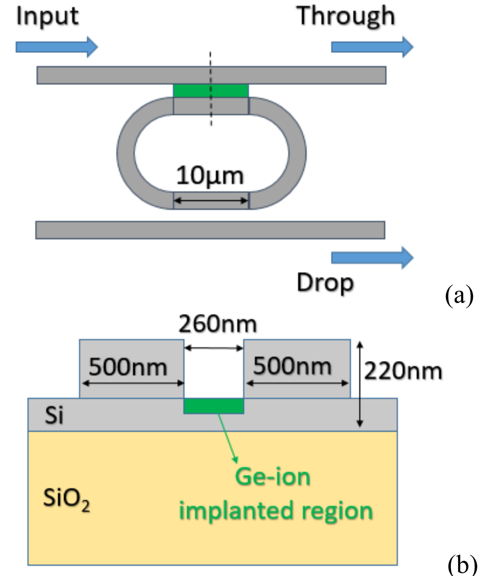

Fig. 1: (a) A schematic of a racetrack resonator and (b) a cross-sectional view of the device.

Silicon-on-insulator rib waveguides and racetrack resonators were fabricated by electron beam lithography and inductively coupled plasma etching following the same procedure as described in Ref. [13]. Figure 2 shows an optical microscope image of a fabricated racetrack resonator. A protective layer of 20 nm thick PECVD oxide was deposited on top of the devices. In the next fabrication step the electron beam resist was deposited as mask layer for ion implantation process. Germanium ion implantation was used to create lattice damage in the silicon slab layer located between the bus waveguide and the racetrack. The ion energy and fluence of 130 keV and 1×10^{15} ions/cm^2 were used, respectively. According to our previously achieved results [1, 2], this process will provide optimum parameters for complete amorphisation of 100 nm thick silicon slab layer. The Germanium peak concentration was about 1.5×10^{20} cm^{-3} (crystalline silicon atomic density is 5×10^{22} cm^{-3} at 25 °C, SOITEC wafers), according to simulation analysis using Silvaco software [16]. The ion implantation process will introduce 80% lattice disorder in silicon, which is

considered as the threshold value for silicon amorphisation, leading to a refractive index increase on the order of 0.5 [1, 2]. A bulk silicon sample was also implanted and served for ellipsometry measurements of the refractive index as detailed in Ref. [1]. It was found that the refractive index of implanted silicon was about 3.96 at the wavelength of 1550 nm. The germanium ion concentration was negligible in comparison to the concentration of silicon ions in the same volume (0.3% at its peak value).

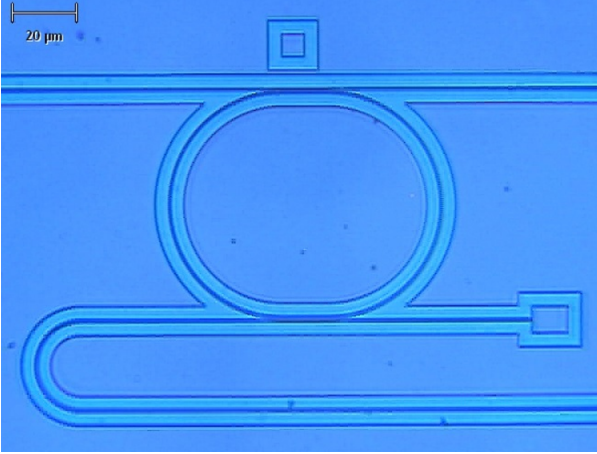

Fig. 2: An optical microscope image of the fabricated racetrack resonator.

Figure 3 shows transmission spectrum of un-implanted racetrack resonators comparing the performance between simulation and experimental results. As can be seen, good agreement with experimental results was achieved. A free-spectral range of ~3.4 nm and extinction ratios greater than 25 dB were obtained in both cases. A difference within 0.5 nm in the target resonant wavelength peak position (1549.8 nm simulated, 1550.3 nm measured) and 1 dB difference in insertion losses (0.89 dB simulated, 1.83 dB measured at 1550 nm) can be associated with errors in the fabrication process and SOI wafer thickness variations. The quality factors of Q=1800 (full width at half maximum, FWHM, of 0.85 nm) and Q=1350 (FWHM of 1.15 nm) were obtained for simulated and measured racetrack resonators at 1550 nm wavelength, which is in a good agreement with our previous results on ring resonators (where a quality factor of Q=1400 was obtained) [13].

III. EXPERIMENTAL RESULTS

Fabricated devices were characterized using Keysight technologies lightwave multimeter (8163B) with a wavelength range from 1520 to 1620 nm. A sample stage with a Peltier element was used to maintain a constant temperature during measurements (20 °C). Shallow etched grating couplers (70 nm etch depth, 630 nm period, 50% duty cycle) were positioned at the input and output of the waveguides to enable efficient coupling of TE polarised light from and to single-mode optical fibers used for characterisation. In all experiments, we tried to minimise any measurement uncertainties that might be a consequence of fabrication imperfections. Therefore, we used a

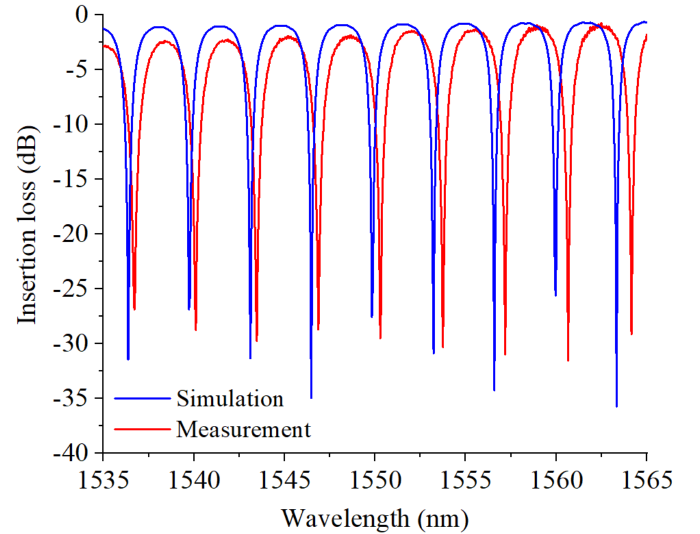

Fig. 3: Transmission spectrum showing the comparison between simulation and experimental results of un-implanted racetrack resonators.

high precision electron beam lithography tool for device fabrication and we kept all devices close to each other on the wafer. This procedure ensured low influence of SOI wafer thickness variations and small device width variations on the transmission spectra from various waveguides and racetrack resonators. Although our simulation analysis revealed 0.5 nm difference between theoretical and measured resonant peak position, experimental results, performed for a series of adjacent racetrack resonators on the same chip, revealed up to 3 nm variation in the resonant wavelength peak position (and 5 dB difference in the extinction ratio). This result demonstrates how highly sensitive these devices are to fabrication imperfections, and therefore the requirement for trimming after fabrication. We have used both continuous and pulsed wave lasers to trim fabricated devices. As reported in our previous research [1, 13-16], laser annealing re-crystallizes the implanted silicon material and gradually reduces its refractive index (from 3.96 to approximately 3.47). This process can be controlled by adjusting the laser power and scanning speed, thus optimizing the extinction ratio of the racetrack resonators.

A. Localised continuous wave laser annealing

The continuous wave laser annealing setup is depicted in Fig. 4. It comprises of 488 nm argon ion laser, half-wave plate and a polarization beam splitter [13, 19]. A 20× microscope objective was used to focus the laser beam onto the sample top surface, producing a spot with 2.5 µm diameter. CCD camera and micro-precision stages were used for imaging and precise control of the laser beam. Depending on the power and a scanning speed of the laser amorphous silicon material can be partially re-crystallised to different extents, modifying its refractive index. According to our recent study [13], the local on chip temperature at which this local change in the refractive index occurs is about 450-500 °C.

We have performed Raman spectroscopy for sample annealed at three different power levels of annealing laser (25 mW, 35 mW and 45 mW) while keeping the scanning speed constant at 10 µm/s. The measurement was taken with a ×50

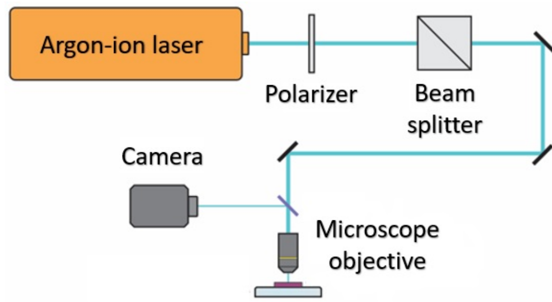

Fig. 4: Experimental setup used for continuous wave laser annealing.

objective lens using a 0.2 mW Nd:YAG laser source (532 nm), an exposure time of 10 s, and an accumulation over 3 exposures. Experimental results are shown in Fig. 5. Broad peaks at 150 cm^{-1} and 470 cm^{-1} confirmed that the amorphous silicon had been successfully formed prior to laser annealing. The laser power of 25 mW was insufficient to provide full re-crystallization of the silicon material, which is confirmed by the broad peak at 150 cm^{-1}. Nevertheless, a silicon peak was also observed at 520 cm^{-1}. Higher laser power of 35 mW and 45 mW revealed a single silicon peak at 520 cm^{-1}. Upon close inspection, a small germanium peak is visible at 300 cm^{-1}, however this did not affect the optical performance of the devices.

Experimental results revealed material absorption loss of 300 dB/cm, which was in agreement with our previous work on ion implantation [13-16]. We have carried out propagation loss measurements of germanium ion implanted waveguides (implanted into the silicon slab) and obtained results in the range between 280 dB/cm and 320 dB/cm before laser annealing which is in good agreement with the measured quality factor of our resonators. As it is customary, the material absorption losses and the losses of Ge-ion implanted waveguides are expressed in dB/cm, and therefore appear to be very high. However, since the length of ion implantation section is very short (up to 10 µm), maximum insertion losses due to implantation are up to 0.32 dB prior to trimming, and reduces accordingly after trimming. Similar to our previous work [13-16], we have also carried out propagation loss measurements for both partially and fully annealed waveguides. Propagation losses lower than 100 dB/cm were measured after partial annealing while fully annealed waveguides showed similar losses to standard un-implanted rib waveguides. This demonstrated that optical losses originate from the amorphisation of the crystalline silicon, not the germanium concentration.

Figure 6 are transmission spectrum of un-implanted and ion implanted racetrack resonators as a function of annealing length. Two different power levels (35 mW and 45 mW) of the continuous wave (CW) Ar-ion laser have been used. These power levels of the annealing laser are in very good agreement with the one used in our previous work on ion implantation [13], and it provides similar refractive index change as the rapid thermal annealing technique used to characterize the effect of temperature (in the temperature range of 450-500 °C carried for 1 min). As can be seen from Fig. 6, the critical coupling of the racetrack resonators can be achieved with this technique. We have obtained a range of different extinction ratios as a function

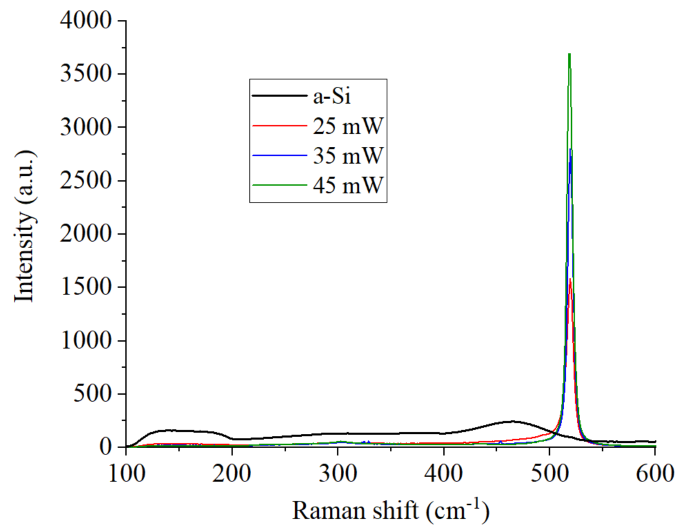

Fig. 5: Raman spectra of Ge implanted silicon before (a-Si) and after annealing using three different power levels of the annealing laser.

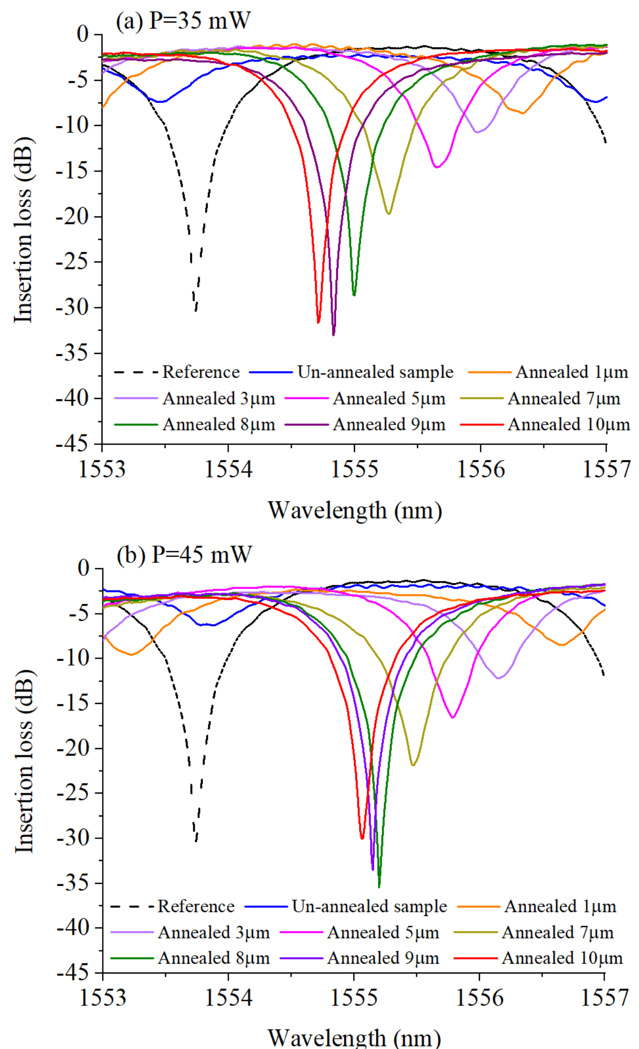

Fig. 6: Transmission spectra of fabricated racetrack resonators as a function of annealing length at: (a) 35 mW and (b) 45 mW power of annealing laser. Reference label corresponds to an un-implanted racetrack resonator.

of annealing length and the laser power level used for annealing. Annealing lengths of 8 µm and 9 µm resulted in an increase of the extinction ratio. An extinction ratio of around 28 dB was measured before annealing (un-implanted racetrack resonator - Reference), however 30 dB and 34 dB were measured for annealing lengths of 9 µm and 8 µm, respectively (which corresponded to the laser power of 35 mW and 45 mW). An increase in extinction ratio was obtained due to critical coupling control of the racetrack resonator. Ge-ion implantation and subsequent laser annealing enabled tuning of the coupling coefficients by modifying the material's refractive index in the silicon slab layer between the bus waveguide and the racetrack resonator. At a certain length of the annealed section, the cross-coupling coefficient matched the round-trip loss of the resonator, allowing for an increase in the extinction ratio. We have performed simulation analysis, using the approach described in Ref. [17], to fit the measurement data, and to estimate trimming range of the average-coupling coefficient (k_{av}) between the bus waveguide and the racetrack (Fig. 7). Good agreement between theoretical and simulation results was obtained. The coupling coefficient ranged between 0.63 and 0.90 which corresponds to a coupling power coefficient (k_{av}^2) of about 0.40 to 0.81, which is dependent on the original coupling strength of the coupler (k'^2_{av}=0.79). The optimum coupling coefficient was found to be equal to ~0.894 (corresponding to a coupling power coefficient of ~0.8).

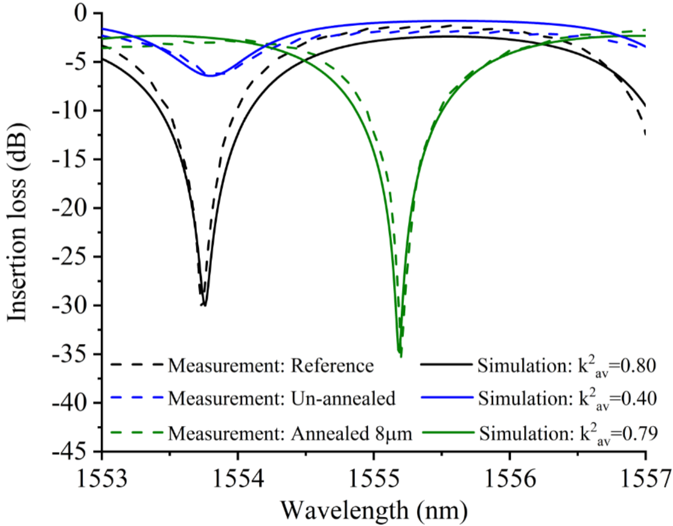

Fig. 7: Transmission spectra of fabricated and simulated racetrack resonators at different annealed lengths and average coupling power coefficients. The power of annealing laser was 45 mW.

Besides improving the extinction ratio of the racetrack resonator, this technique also caused a resonant wavelength shift, which is usually undesirable in integrated photonic systems. However, the measured resonant wavelength shift of 1 nm is relatively small and is comparable to the wavelength shift caused by ambient temperature fluctuations of 10 °C (assuming a wavelength shift of 100 pm/K) [3]. Furthermore, this wavelength shift could be trimmed actively in combination with our previously reported ion-implanted post-fabrication trimming technique [13], in which we formed a short ion-

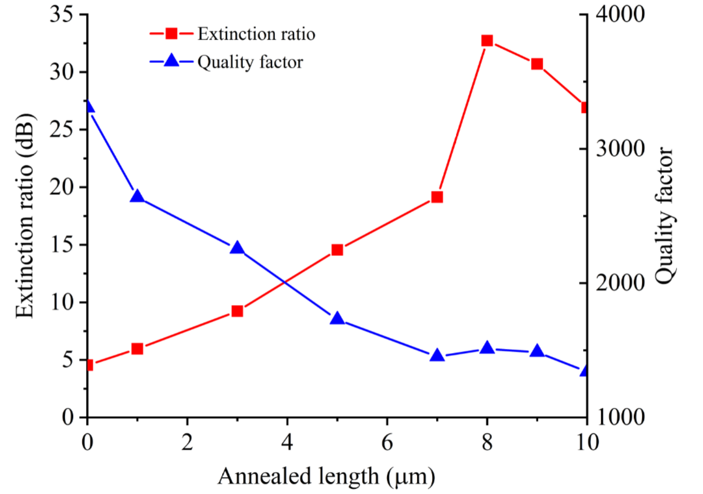

Fig. 8: Extinction ratio and quality factor as a function of annealed length for the annealing laser power of 45 mW.

implanted section in the silicon waveguide arc of the resonator and used localised laser annealing to precisely control the operating wavelength of this device. Thus, we can control both the resonant wavelength and the critical coupling condition of the ring resonator. The quality factor of our racetrack resonators after laser annealing was Q=1510 (FWHM of 1.03 nm at 1555.2 nm wavelength) and Q=1600 (FWHM of 0.97 nm at 1554.83 nm wavelength) for an annealed length of 8 µm (45 mW) and 9 µm (35 mW), respectively, which is in a good agreement with the quality factor of un-implanted racetrack resonators (Q=1260, FWHM of 1.23 nm at 1553.74 nm wavelength). The resonators revealed relatively low-quality factors due to the presence of a drop-port in our initial design. The results from Fig. 6 also showed that ion implantation of the 10 µm long silicon slab layer only induced very little additional loss (<0.2 dB) compared to un-implanted racetrack resonators, therefore, demonstrating that the Ge-ion concentration implanted into silicon slab, had a negligible effect on the quality factor. Figure 8 shows the extinction ratio and quality factor as a function of annealed length for the annealing laser power of 45 mW. As can be seen, at critical coupling, the extinction ratio reaches its maximum (annealed length of 8 µm), whilst quality factor changes accordingly.

Due to relatively low quality factor of the example racetrack resonators used in this work, we have not observed any backscattering of light, which may in turn, cause splitting of the resonant wavelength peak. This effect typically occurs in ultra-high Q optical filters [20] and is undesirable in many applications (e.g. sensing, wavelength-division multiplexing filters), however, in some situations may provide attractive benefits (e.g. strengthening the extinction ratio of optical filters) [20]. The resonance splitting is induced by sidewall roughness and coupler induced backscattering [20]. Ion implantation of the silicon slab layer and laser annealing induce an abrupt change in the silicon refractive index, which may lead to reflections at Si/a-Si interface. However, ion implantation of a longer region and precise control of laser annealing with variable laser power may provide a graded index tapering of the material's refractive index and therefore, reduce the possibility

for wavelength splitting in high-Q resonant filters.

B. Localised pulsed wave laser annealing

Similar to our previous analysis for real-time resonant wavelength trimming [15], we have also investigated the possibility for trimming the extinction ratio of racetrack resonators using pulsed laser sources.

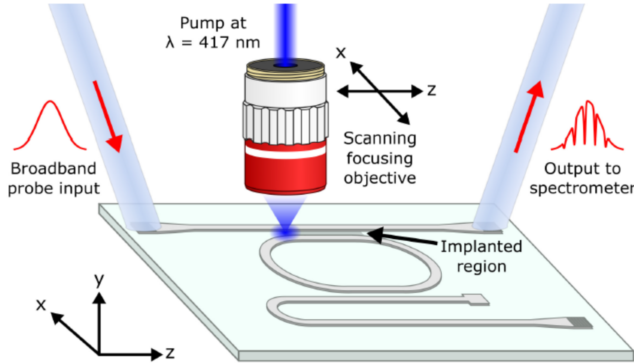

Fig. 9: Experimental setup used for pulsed-wave laser annealing.

Figure 9 shows an illustration of the experimental setup. A 200 fs mode-locked Ti:Sapphire laser (Coherent Chameleon Ultra II) operating at 80 MHz was used in conjunction with an optical parametric oscillator (Coherent Chameleon Compact OPO) to produce the broadband probe pulse centred around 1550 nm wavelength with a 20 nm bandwidth. The second harmonic of the 834 nm wavelength seed pulse provided the pump beam at 417 nm, which was externally focused onto the surface of the device using a 100× objective (Mitutoyo) with a numerical aperture of 0.5. This resulted in FWHM spot size of 740 nm at the focus with an average power of 5 mW. The focusing objective was mounted to a 3D piezo nanopositioner (SmarAct), allowing the pump spot to be scanned over the implanted region, while the output of the device was analysed using a grating spectrometer equipped with an InGaAs CCD array (Andor) providing 0.13 nm spectral resolution. This arrangement offers the advantage of fast monitoring of the response during the annealing. However, the combination of spectral resolution and background scattering in the broadband spectroscopy setup resulted in available dynamic measurement range of 16 dB, lower than obtained using a swept-wavelength source (80 dB). A shutter placed in the pump beam removed any free-carrier or thermal contributions during the measurement of the spectrum. The focusing objective was also used for imaging and alignment purposes.

Figure 10 shows the measured resonant wavelength shift and extracted transmission spectrum of fabricated racetrack resonator at different annealing lengths using the 5 mW pulsed laser. Similar to annealing using continuous wave lasers, this technique also resulted in a small wavelength shift of 1 nm and an increase in racetrack resonator extinction ratio (11 dB). Due to the real-time monitoring system, we were able to obtain more precise information about the required annealing length in order to achieve optimal performance. The annealing length of 9.5 µm was sufficient to provide 11 dB extinction ratio of the racetrack resonator. The curve saturates at an implantation length of 10 µm because at this point the overall length of the Ge-ion implanted section was fully annealed (Fig. 10c). The quality factor of our racetrack resonator after pulsed wave laser annealing was Q=1500 (FWHM of 1.07 nm at 1552.9 nm wavelength) which is slightly higher than the quality factor before laser annealing (Q=1260).

While the average intensity over the spot size was comparable for both the pulsed and the CW experiments, some notable differences were observed between the two regimes. In particular, the extinction ratio of the spectral dip is a lot smaller

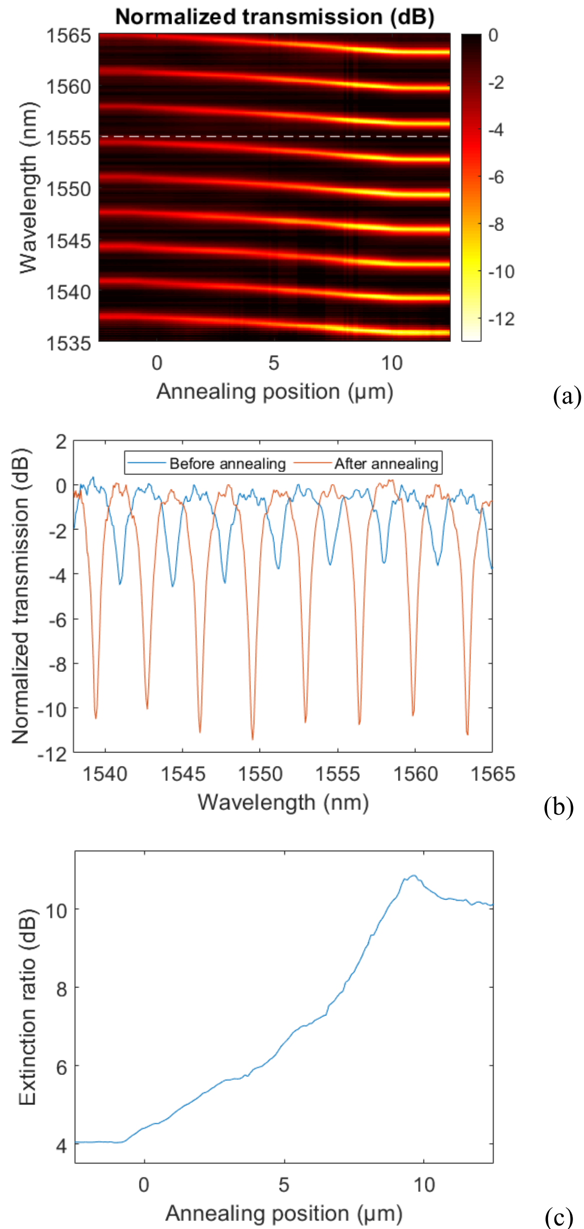

Fig. 10: (a) Measured resonant wavelength shift of fabricated racetrack resonators as a function of different annealing position using 5 mW of pulsed laser power. (b) Extracted transmission spectra of fabricated racetrack resonators before and after pulsed wave laser annealing. (c) Extinction ratio of fabricated racetrack resonators as a function of annealing position using 5 mW of pulsed laser power. Optimal annealing length was found at around 9.5 µm.

in the case of annealing using the pulsed laser than for CW annealing. The limited extinction ratio was confirmed by swept source measurements (not shown). The extinction at critical coupling is very sensitive to scattering generated by imperfections in the device and it may be that different re-crystallization conditions result in different quality of the silicon. In particular, pulsed annealing involves fast dynamics which does affect the crystallization process. To further investigate the effect of pulsed annealing on the quality of the re-crystalisation, we show in Fig. 11 the Raman spectrum from a pulsed annealing experiment using the same conditions as in Fig. 10. As can be seen, in all cases, pulsed laser power was insufficient to provide full re-crystallization of Ge-ion implanted silicon which is confirmed by broad peaks at 500 cm^{-1}. Thus, the pulsed laser annealing did not provide a complete silicon re-crystallization which could explain a reduced extinction ratio found for this device.

The use of localised laser annealing, described in this paper and in our previous work [13-16], and integrated micro-heater annealing (such as Refs. [9, 10]) are very important for post fabrication trimming of silicon photonics optical filters. Both approaches advantageously provide significant reduction in the overall power consumption that is necessary to compensate for optical signal degradations caused by device fabrication uncertainties and wafer thickness variations. Both processes are also CMOS compatible and share very similar fabrication complexity and costs. Although ion implantation and laser-trimming technique requires no fabrication step for electrical heaters fabrication, it may add up to the overall trimming complexity. While localised laser annealing provides the possibility for precise localization and control of the trimming accuracy, electrical annealing is commercially appealing and is expected to become mainstream in silicon photonics. However, whilst electrical annealing is desirable, it constrains flexibility in the annealing process, if, for example, only part of the implanted region is to be annealed, multiple heaters would clearly be more complex than a single laser scan. The optimum solution may be a combination of both approaches.

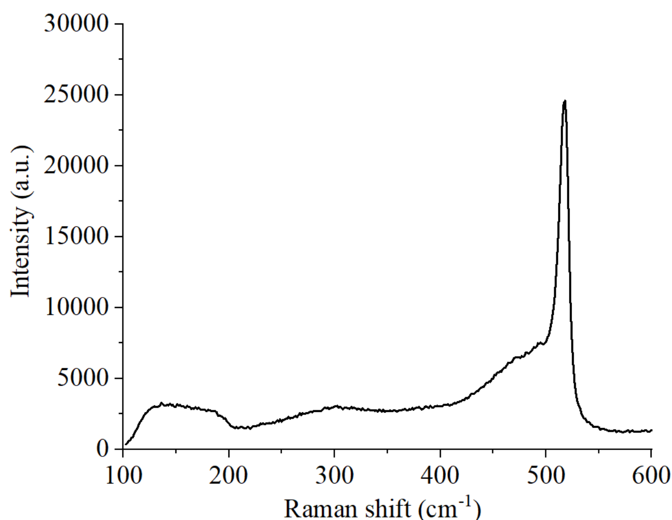

Fig. 11: Raman spectra of Ge-ion implanted silicon annealed using pulsed laser.

IV. CONCLUSION

Silicon photonics racetrack resonators represent a fundamental building component of photonic circuits, however their optical response is very sensitive to fabrication imperfections. In this paper, we have performed simulation and experimental analysis of trimming the critical coupling of these devices using germanium ion implantation followed by localised laser annealing. Experimental results revealed that localised annealing of germanium implanted section using continuous wave lasers can be used to permanently tune the critical coupling of this device. It can be performed relatively quickly and it involves the possibility for trimming each device on the chip separately without affecting the whole optical circuit. Therefore, it is highly attractive for practical applications. Localised annealing using pulsed wave laser sources gives us more precise information about the required annealing length than the localised continuous wave laser annealing, however it decreases the extinction ratio due to a poorer material quality after silicon recrystallization. Nevertheless, pulsed laser annealing can be fully used for real-time resonant wavelength trimming of optical filters. This technology is CMOS compatible and can be adapted to advance emerging platforms and systems such as multilayer programmable photonics.

ACKNOWLEDGMENT

This work was funded by EPSRC project under the “Silicon Photonics for Future Systems” (EP/L00044X/1), “Electronic-Photonic convergence” (EP/N013247/1), “Laser-Engineered Silicon” (EP/M022757/1) and “CORNERSTONE” (EP/L021129/1) projects. Reed is a Royal Society Wolfson Research Merit Award holder. He is grateful to the Wolfson Foundation and the Royal Society for funding of the award. Thomson is grateful to the Royal Society for funding. Yu acknowledges funding from the Scholarship Council of China. The dataset related to this paper is accessible from https://doi.org/10.5258/SOTON/D1170.

References

1. R. Topley, L. O’Faolain, D. J. Thomson, F. Y. Gardes, G. Z. Mashanovich, and G. T. Reed, “Planar surface implanted diffractive grating couplers in SOI,” *Opt. Express*, vol. 22, pp. 1077-1084, 2014.

2. R. Topley, G. Martinez-Jimenez, L. O’Faolain, N. Healy, S. Mailis, D. J. Thomson, F. Y. Gardes, A. C. Peacock, D. N. R. Payne, G. Z. Mashanovich, and G. T. Reed, “Locally erasable couplers for optical device testing in silicon on insulator,” *Journal of Lightw. Technol.*, vol. 32, no. 12, pp. 2248-2253, 2014.

3. M. M. Milosevic, N. G. Emerson, F. Y. Gardes, X. Chen, A. A. D. T. Adikaari, G. Z. Mashanovich, “Athermal waveguides for optical communication wavelengths,” *Opt. Lett.*, vol. 36, no. 23, pp. 4659-4651, 2011.

4. G. T. Reed, G. Mashanovich, F. Y. Gardes, D. J. Thomson, “Silicon optical modulators,” *Nat. Photon.,* vol. 4, pp. 518-526, 2010.

5. K. Padmaraj, K. Bergman, “Resolving thermal challenges for silicon microring resonator devices,” *Nanophoton.,* vol. 3, no. 4-5, pp. 269-281, 2014.

6. L. Yu, Y. Yin, Y. Shi, D. Dai, S. He, “Thermally tunable silicon photonic microdisk resonator with transparent graphene nanoheaters,” *Optica*, vol. 3, no. 2, pp. 159-166, 2016.

7. J. Schrauwen, D. Van Thourhout, and R. Baets, “Trimming of silicon ring resonator by electron beam induced compaction and strain,” *Opt. Express,* vol. 16, pp. 3738-3743, 2008.

8. S. Prorok, A. Y. Petrov, M. Eich, J. Luo, and A. K.-Y. Jen, “Trimming of high-Q-factor silicon ring resonators by electron beam bleaching,” *Opt. Lett.*, vol. 37, pp. 3114-3116, 2012.

9. S. Spector. J. M. Knecht, and P. W. Juodawlkis, "Localised *in situ* cladding annealing for post-fabrication trimming of silicon photonic integrated circuits," *Opt. Express*, vol. 24, no. 6, pp. 5996-6003, 2016.
10. D. E. Hagan, B. Torres-Kulik, and A. P. Knights, "Post-fabrication trimming of silicon ring resonators via integrated annealing," *IEEE Photon. Techol. Lett.*, vol. 31, no. 16, pp. 1373-1376, 2019.
11. X. Chen, M. M. Milosevic, S. Stankovic, S. Reynolds, T. D. Bucio, K. Li, D. J. Thomson, F. Y. Gardes, G. T. Reed, „The emergence of silicon photonics as a flexible technology platform," *Proc. of the IEEE*, vol. 106, no. 12, pp. 2101-2116, 2018.
12. J. J. Ackert, J. K. Doylend, D. F. Logan, P. E. Jessop, R. Vafaei, L. Chrostowski, A. P. Knights, "Defect-mediated resonance shift of silicon-on-insulator racetrack resonators," *Opt. Express,* vol. 19, no. 13, pp. 11970-11976, 2011.
13. M. M. Milosevic, X. Chen, W. Cao, A. F. J. Runge, J. Franz, C. G. Littlejohns, S. Mailis, A. C. Peacock, D. J. Thomson, G. T. Reed, "Ion Implantation in Silicon for Trimming the Operating Wavelength of Ring Resonators," *IEEE J. Sel. Top. In Quan. Electr.,* vol. 24, no. 4, 8200107, 2018.
14. X. Chen, M. M. Milosevic, D. J. Thomson, A. Z. Khokhar, J. Franz, A. F. J. Runge, S. Mailis, A. C. Peacock, G. T. Reed, "Post-fabrication phase trimming of Mach-Zehnder interferometers by laser annealing of germanium implanted waveguides," *Photon. Research,* vol. 5, no. 6, pp. 578-582, 2017.
15. B. Chen, X. Yu, X. Chen, M. M. Milosevic, D. J. Thomson, A. Z. Khokhar, S. Saito, O. L. Muskens, G. T. Reed, "Real-time monitoring and gradient feedback enable accurate trimming of ion-implanted silicon photonic devices," *Opt. Express,* vol. 26, no. 19, pp. 24953-24963, 2018.
16. X. Chen, M. M. Milosevic, A. F. J. Runge, X. Yu, A. Z. Khokhar, S. Mailis, D. J. Thomson, A. C. Peacock, S. Saito, G. T. Reed, "Towards an optical FPGA - Programmable silicon photonic circuits," *arXiv:1807.01656 (Optics)*, 2018.
17. W. Bogaerts, P.D. Heyn, T. V. Vaerenbergh, K. D. Vos, S. K. Selveraja, T. Claes, P. Dumon, P. Bienstman, D. V. Thourhout, R. Baets, "Silicon microring resonators," *Laser Photonic Rev.*, vol. 6, no. 1, pp. 47-73, 2012.
18. www.lumerical.com
19. N. Healy, S. Mailis, N. M. Bulgakova, P. J. A. Sazio, T. D. Day, J. R. Sparks, H. Y. Cheng, J. V. Badding, and A. C. Peacock, "Extreme electronic bandgap modification in laser-crystallized silicon optical fibres," *Nat. Mater.*, vol. 13, pp. 1122-1127, 2014.
20. A. Li, T. V. Vaerenbergh, P. D. Heyn, P. Bienstman, and W. Bogaerts, „Backscattering in silicon microring resonators: a quantitative analysis," *Laser Photon. Rev.*, vol. 10, no. 3, pp. 420-431, 2016.